

We are IntechOpen, the world's leading publisher of Open Access books Built by scientists, for scientists

5,800

Open access books available

142,000

International authors and editors

180M

Downloads

Our authors are among the

154

Countries delivered to

TOP 1%

most cited scientists

12.2%

Contributors from top 500 universities



WEB OF SCIENCE™

Selection of our books indexed in the Book Citation Index
in Web of Science™ Core Collection (BKCI)

Interested in publishing with us?
Contact book.department@intechopen.com

Numbers displayed above are based on latest data collected.
For more information visit www.intechopen.com



Wireless Power Transmission on Biomedical Applications

Ting-Wei Wang and Ting-Tse Lin

Abstract

Wireless power transmission (WPT) can provide an alternative for wireless power in implantable medical devices (IMDs). The WPT in implantable medical devices will involve many emerging biomedical topics, such as implantable pacemakers, optogenetic devices, and bio-impedance sensors. To this end, this chapter comprehensively reviews the recent WPT studies for those mentioned above emerging biomedical applications. The specific key components are carried out for those applications. Besides, the operation principle and system design are presented. In conclusion, this chapter's significance can help evolve reliable implantable device development in the future.

Keywords: bio-impedance sensor, electrical field coupling, implantable medical devices, magnetic field coupling, optogenetic device, pacemaker, resonance circuit

1. Introduction

Wireless power transmission (WPT) is an emerging technology to transmit power without wires [1, 2]. It is widely studied in various applications such as consumer electronics charging [3], radio-frequency identification (RFID) system [4], electric vehicle charging [5], biomedical applications [6], etc. Especially in implantable devices, the market benefit of global implantable medical devices achieved a value of US\$ 120.5 billion in 2021 by IMARC Group. The market can be expected to reach US\$ 168.3 billion by 2027, exhibiting at a compound annual growth rate (CAGR) of 5.54% during 2022–2027. In practice, implantable devices solve today's problems using advanced medical technologies such as a well-known pacemaker and capsule endoscopy [7, 8]. The pacemaker and capsule endoscopy invention brings new perspectives for cardiovascular disease therapy and direct health diagnosis of the whole small bowel. Although several miniaturized battery systems have been developed to provide several years of power supply for implantable devices, a battery replacement would induce patients' inconvenient and unexpected surgery risks [9, 10]. Recently, the WPT technique has been widely applied in implantable medical devices that are expected to power supply issues in the future [11, 12].

WPT technique can be mainly divided into the coupling and radiative approaches [13, 14], as shown in **Figure 1**. The WPT coupling can be categorized into magnetic and electric field methods. The radiative approach can be categorized into

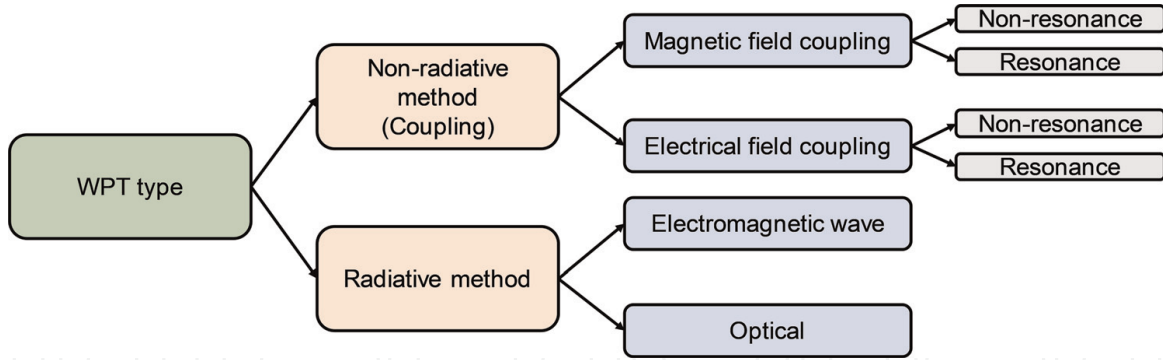


Figure 1. WPT classification, including nonradiative and radiative methods.

electromagnetic waves and optical power transmission. In the radiative method (far-field), power is transferred by electromagnetic radiation in terms of microwave, laser, and light. Although radiative techniques can transfer power over longer distances, the large environmental loss-induced transfer efficiency is considerable due to poor air medium. The nonradiative method (near field) utilizes magnetic field and electric field coupling to approach wireless power transfer. The main advantage of nonradiative techniques is high transfer efficiency; however, its technical limitation is that the transfer distance is limited.

The nonradiative method is also called coupling-based WPT, which can be described as the power-transmitting side (primary side) and power-receiving side (secondary side). The coupling type can be classified as a magnetic field (**Figure 2a**) and electrical field coupling (**Figure 2b**). Both magnetic and electric field coupling methods can be further categorized as resonance mode, based on LC resonance (**Figure 2c and d**).

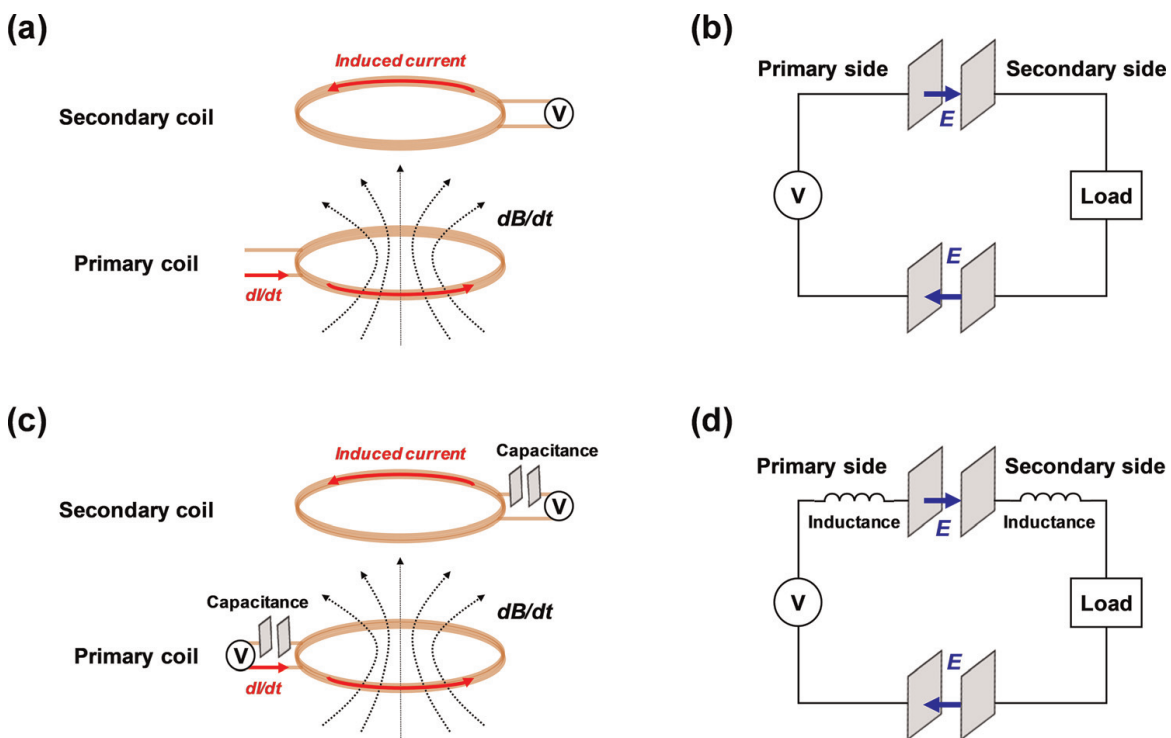


Figure 2. Magnetic and electric field coupling with and without resonant circuit.

2. Magnetic field coupling without resonance

The magnetic field coupling without resonance type utilizes the principle of electromagnetic induction, as shown in **Figure 3**. According to Ampere's law as Eq. (1), the magnetic pulsing ($d\mathbf{B}/dt$) of the primary coil can be generated by time-varying driving current (dI/dt). Where \mathbf{B} , μ_0 , \mathbf{J} are magnetic field, permeability, and current density. The electric field \mathbf{E} can be induced on the secondary coil, according to Faraday's law as Eq. (2) [9, 15]. Thus, the charge can be stored *via* a secondary coil.

$$\nabla \times \mathbf{B} = \mu_0 \mathbf{J} \quad (1)$$

$$\mathbf{E} = -\frac{\partial \mathbf{B}}{\partial t} \quad (2)$$

To understand the principle of magnetic field coupling without resonance, **Figure 3** shows the topology of the circuit analysis. The mutual inductance, $L_m = k\sqrt{L_1 L_2}$, depends on the distance x between the two coils, where k is the coupling factor ($0 < k < 1$) between the primary and the secondary coil. Based on Kirchhoff's voltage law, Eqs. (3) and (4) can be obtained as below [16]:

$$j\omega L_1 I_1 + I_1 R_1 + j\omega L_m I_2 = U_1 \quad (3)$$

$$j\omega L_2 I_2 + I_2 R_2 + I_2 R_L + j\omega L_m I_1 = 0 \quad (4)$$

I_2 can be expressed as Eq. (5), according to Eq. (4).

$$I_2 = -I_1 \left[\frac{\omega L_m}{\omega L_2 - j(R_2 + R_L)} \right] \quad (5)$$

The relation between I_1 and U_1 can be obtained as Eq. (6), according to Eqs. (3) and (5).

$$I_1 = \left[\frac{R_2 + R_L + j\omega L_2}{(R_1 + j\omega L_1)(j\omega L_2 + R_2 + R_L) + \omega^2 L_m^2} \right] U_1 \quad (6)$$

The relation between I_1 and I_2 can be expressed as Eq. (7), according to Eqs. (5) and (6).

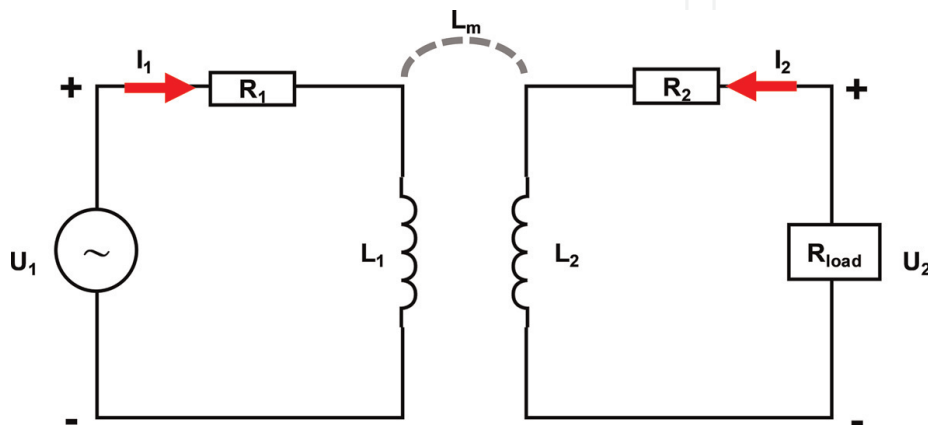


Figure 3.
 Circuit topology of electromagnetic induction.

$$I_2 = - \left[\frac{j\omega L_m}{(R_1 + j\omega L_1)(j\omega L_2 + R_2 + R_L) + \omega^2 L_m^2} \right] U_1 \quad (7)$$

The ratio of I_1 and I_2 can be expressed as Eq. (8), according to Eqs. (6) and (7).

$$\frac{I_1}{I_2} = - \frac{R_2 + R_L + j\omega L_2}{j\omega L_m} \quad (8)$$

To better understand the input impedance and power efficiency of the circuit, a T-type equivalent circuit is used in **Figure 4**.

$$V_{Lm2} = j\omega L_m I_1 \quad (9)$$

$$V_{Lm2} = \frac{j\omega L_m (R_2 + R_L + j\omega L_2)}{(R_1 + j\omega L_1)(j\omega L_2 + R_2 + R_L) + \omega^2 L_m^2} U_1 \quad (10)$$

According to Eq. (11), Z_{in2} can be obtained from Eqs. (8) and (9).

$$Z_{in2} = \frac{V_{Lm2}}{-I_2} = \frac{j\omega L_m I_1}{-I_2} = R_2 + R_L + j\omega L_2 \quad (11)$$

Then, Z_2 can be further obtained, according to Eq. (12).

$$Z_2 = \frac{V_{Lm1}}{I_1} = \frac{j\omega L_m I_2}{I_1} = \frac{\omega^2 L_m^2}{R_2 + R_L + j\omega L_2} \quad (12)$$

Finally, the Z_{in1} can be acquired, according to Eq. (13).

$$Z_{in1} = R_1 + j\omega L_1 + Z_2 = R_1 + j\omega L_1 + \frac{\omega^2 L_m^2}{R_2 + R_L + j\omega L_2} \quad (13)$$

To understand the power efficiency, the energy loss ratio for the primary-side internal resistance, secondary resistance, and load can be denoted by P_{R1} , P_{R2} , and P_{RL} as Eq. (14).

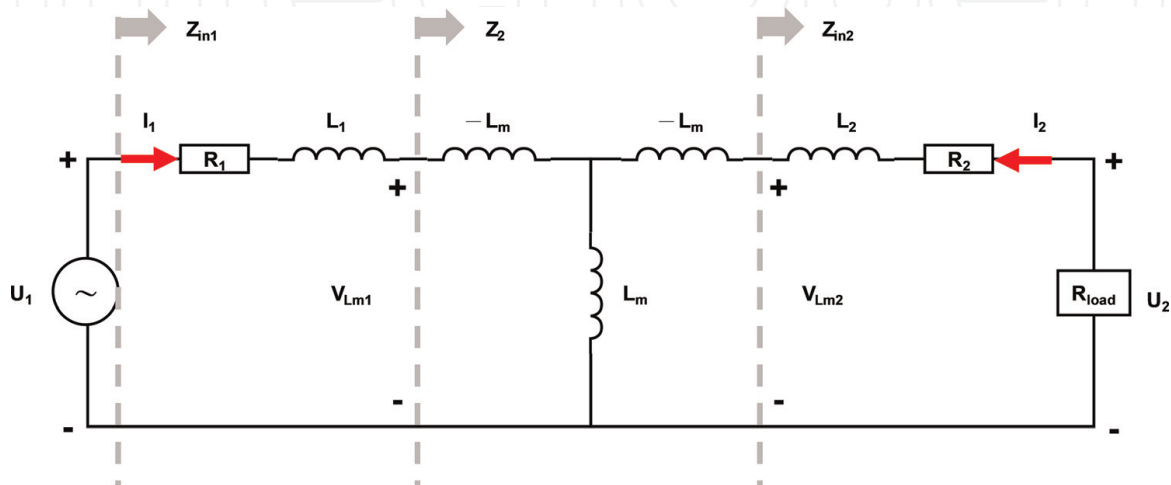


Figure 4.
T-type equivalent circuit for electromagnetic induction.

$$P_{R_1} : P_{R_2} : P_L = |I_1|^2 R_1 : |I_2|^2 R_2 : |I_2|^2 R_L \quad (14)$$

The square ratio of I_2 and I_1 can be expressed as Eq. (15), according to Eq. (8)

$$\left| \frac{I_2}{I_1} \right|^2 = \frac{\omega^2 L_m^2}{(R_2 + R_L)^2 + \omega^2 L_m^2} \quad (15)$$

The power ratio can be rewritten as Eq. (16), according to Eqs. (14) and (15).

$$P_{R_1} : P_{R_2} : P_L = \left\{ (R_2 + R_L)^2 + \omega^2 L_m^2 \right\} R_1 : \left\{ \omega^2 L_m^2 \right\} R_2 : \left\{ \omega^2 L_m^2 \right\} R_L \quad (16)$$

Finally, the power efficiency can be obtained, according to Eq. (17).

$$\eta = \frac{P_L}{P_{in}} = \frac{P_L}{P_{R_1} + P_{R_2} + P_L} = \frac{\left\{ \omega^2 L_m^2 \right\} R_L}{\left\{ (R_2 + R_L)^2 + \omega^2 L_m^2 \right\} R_1 + \left\{ \omega^2 L_m^2 \right\} R_2 + \left\{ \omega^2 L_m^2 \right\} R_L} \quad (17)$$

3. Magnetic field coupling with resonance

Compared with electromagnetic induction, magnetic resonance coupling utilizes resonance with the series capacitor in primary and secondary sides to approach high efficiency and high power (**Figure 5**). Based on Kirchhoff's voltage law, Eqs. (18) and (19) can be obtained as below [16]:

$$\frac{1}{j\omega C_1} I_1 + R_1 I_1 + j\omega L_1 I_1 + j\omega L_m I_2 = U_1 \quad (18)$$

$$j\omega L_2 I_2 + R_2 I_2 + \frac{1}{j\omega C_2} I_2 + R_L I_2 + j\omega L_m I_1 = 0 \quad (19)$$

I_2 can be expressed as Eq. (20), according to Eq. (18).

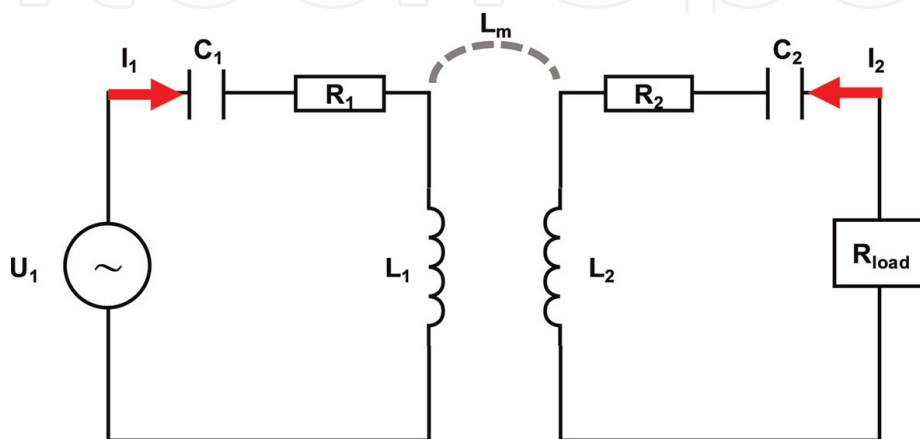


Figure 5.
 Circuit topology of magnetic field coupling with resonance.

$$I_2 = \frac{-j\omega L_m}{j\omega L_2 + \frac{1}{j\omega C_2} + R_2 + R_L} I_1 \quad (20)$$

The relation between I_1 and U_1 can be expressed as Eq. (21), according to Eqs. (18) and (20).

$$I_1 = \left\{ \frac{R_2 + R_L + j\left(\omega L_2 - \frac{1}{\omega C_2}\right)}{\left[\left(R_1 + j\left(\omega L_1 - \frac{1}{\omega C_1}\right) \right) \left[R_2 + R_L + j\left(\omega L_2 - \frac{1}{\omega C_2}\right) \right] + \omega^2 L_m^2} \right\} U_1 \quad (21)$$

The relation between I_2 and U_1 can be expressed as Eq. (22), according to Eqs. (20) and (21).

$$I_2 = - \left\{ \frac{j\omega L_m}{\left[\left(R_1 + j\left(\omega L_1 - \frac{1}{\omega C_1}\right) \right) \left[R_2 + R_L + j\left(\omega L_2 - \frac{1}{\omega C_2}\right) \right] + \omega^2 L_m^2} \right\} U_1 \quad (22)$$

The relation between I_1 and U_1 can be expressed as Eq. (23), according to Eqs. (21) and (22).

$$\frac{I_1}{I_2} = - \frac{R_2 + R_L + j\omega\left(\omega L_2 - \frac{1}{\omega C_2}\right)}{j\omega L_m} \quad (23)$$

When the operating and resonant frequencies are equal on primary and secondary sides, I_1 and I_2 can be expressed as (25) and (26), according to Eqs. (21), (22), and (24).

$$\omega_0 = \omega_1 = \omega_2 = \frac{1}{\sqrt{L_1 C_1}} = \frac{1}{\sqrt{L_2 C_2}} \quad (24)$$

$$I_1 = \frac{R_2 + R_L}{R_1(R_2 + R_L) + \omega^2 L_m^2} U_1 \quad (25)$$

$$I_2 = - \frac{j\omega L_m}{R_1(R_2 + R_L) + \omega^2 L_m^2} U_1 \quad (26)$$

The ratio of I_1 and I_2 can be rewritten as Eq. (27), according to Eqs. (25) and (26).

$$\frac{I_1}{I_2} = - \frac{R_2 + R_L}{j\omega L_m} \quad (27)$$

To further understand the input impedance and power efficiency of the magnetic field coupling with the resonance circuit, a T-type equivalent circuit is used as **Figure 6**.

$$V_{Lm2} = j\omega L_m I_1 \quad (28)$$

$$V_{Lm2} = j\omega L_m \frac{R_2 + R_L}{R_1(R_2 + R_L) + \omega^2 L_m^2} U_1 \quad (29)$$

Z_{in2} can be obtained as Eq. (30), according to Eqs. (26) and (29).

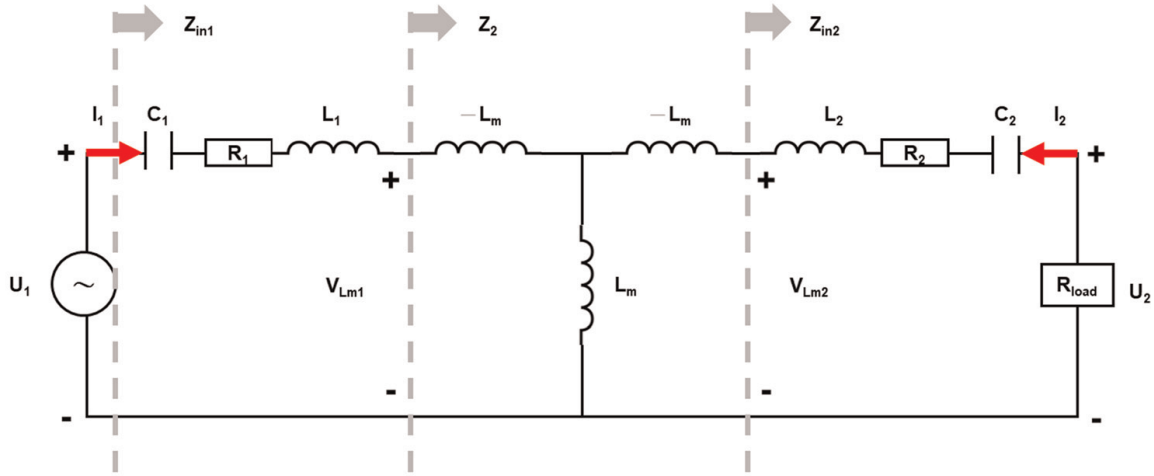


Figure 6.
T-type equivalent circuit for magnetic field coupling with resonance.

$$Z_{in2} = \frac{V_{Lm2}}{-I_2} = \frac{j\omega L_m I_1}{-I_2} = R_2 + R_L \quad (30)$$

Then, Z_2 can be further obtained as Eq. (31).

$$Z_2 = \frac{V_{Lm1}}{I_1} = \frac{j\omega L_m I_2}{I_1} = \frac{\omega^2 L_m^2}{R_2 + R_L} \quad (31)$$

Finally, the Z_{in1} can be acquired, according to Eq. (32).

$$Z_{in1} = R_1 + \frac{1}{j\omega C_1} + j\omega L_1 + Z_2 = R_1 + \frac{1}{j\omega C_1} + j\omega L_1 + \frac{\omega^2 L_m^2}{R_2 + R_L} \quad (32)$$

To understand the power efficiency, the ratio of energy loss for the primary-side internal resistance, secondary resistance, and load can be denoted by P_{R1} , P_{R2} , and P_{RL} as Eq. (14).

$$P_{R1} : P_{R2} : P_L = |I_1|^2 R_1 : |I_2|^2 R_2 : |I_2|^2 R_L \quad (33)$$

The square ratio of I_2 and I_1 can be expressed as Eq. (34), according to Eq. (27).

$$\left| \frac{I_2}{I_1} \right|^2 = \frac{\omega^2 L_m^2}{(R_2 + R_L)^2} \quad (34)$$

The power ratio can be rewritten as Eq. (35), according to Eqs. (33) and (34).

$$P_{R1} : P_{R2} : P_L = \left\{ (R_2 + R_L)^2 \right\} R_1 : \left\{ \omega^2 L_m^2 \right\} R_2 : \left\{ \omega^2 L_m^2 \right\} R_L \quad (35)$$

Finally, the power efficiency can be obtained, according to Eq. (36).

$$\eta = \frac{P_L}{P_{in}} = \frac{P_L}{P_{R1} + P_{R2} + P_L} = \frac{\left\{ \omega^2 L_m^2 \right\} R_L}{\left\{ (R_2 + R_L)^2 \right\} R_1 + \left\{ \omega^2 L_m^2 \right\} R_2 + \left\{ \omega^2 L_m^2 \right\} R_L} \quad (36)$$

	Efficiency	Power at R_{load}
Magnetic field coupling without resonance	$\frac{\{\omega^2 L_m^2\} R_L}{\{(R_2 + R_L)^2 + \omega^2 L_m^2\} R_1 + \{\omega^2 L_m^2\} R_2 + \{\omega^2 L_m^2\} R_L}$	$\left \frac{j\omega L_m}{(R_1 + j\omega L_1)(j\omega L_2 + R_2 + R_L) + \omega^2 L_m^2} \right ^2 U_1^2 R_L$
Magnetic field coupling With resonance	$\frac{\{\omega^2 L_m^2\} R_L}{\{(R_2 + R_L)^2\} R_1 + \{\omega^2 L_m^2\} R_2 + \{\omega^2 L_m^2\} R_L}$	$\left \frac{j\omega L_m}{R_1(R_2 + R_L) + \omega^2 L_m^2} \right ^2 U_1^2 R_L$

Table 1.
Comparison between magnetic field coupling under either no or with resonance.

Table 1 summarizes the results from the previous derivation in terms of the efficiency and power of the two types of magnetic field coupling circuits. With C_1 and C_2 inserted on the primary and secondary sides, the power efficiency and power at R_{load} will increase, which is why resonance is important.

4. Electric field coupling

Compared with magnetic field coupling, the electric field coupling without resonance uses a displacement current instead of an electromagnetic induction (**Figure 7**), as Eq. (37). Where ϵ , E , and D are permittivity, electric field intensity, electric flux density, respectively [17–19].

$$I = \frac{\partial D}{\partial t} \cdot S = \epsilon \frac{\partial E}{\partial t} \cdot S \tag{37}$$

In **Figure 8**, the mutual inductance of C_m between two capacitances on the distance x between the two coils can be written as $C_m = k\sqrt{C_1 C_2}$.

The electrical field coupling schematic diagram can be equivalent to π -type coupling, as shown in **Figure 9**. Based on the mesh-analysis method, the basic mathematical expression can be described as a matrix, according to Eq. (38).

$$\begin{bmatrix} U \\ 0 \\ 0 \end{bmatrix} = \begin{bmatrix} R_1 + j\omega L_1 + \frac{1}{j\omega(C_1 - C_m)} & -\frac{1}{j\omega(C_1 - C_m)} & 0 \\ -\frac{1}{j\omega(C_1 - C_m)} & \frac{1}{j\omega(C_1 - C_m)} + \frac{1}{j\omega C_m} + \frac{1}{j\omega(C_2 - C_m)} & -\frac{1}{j\omega(C_2 - C_m)} \\ 0 & -\frac{1}{j\omega(C_2 - C_m)} & R_2 + R_L + j\omega L_2 + \frac{1}{j\omega(C_2 - C_m)} \end{bmatrix} \begin{bmatrix} I_{11} \\ I_m \\ I_{12} \end{bmatrix} \tag{38}$$

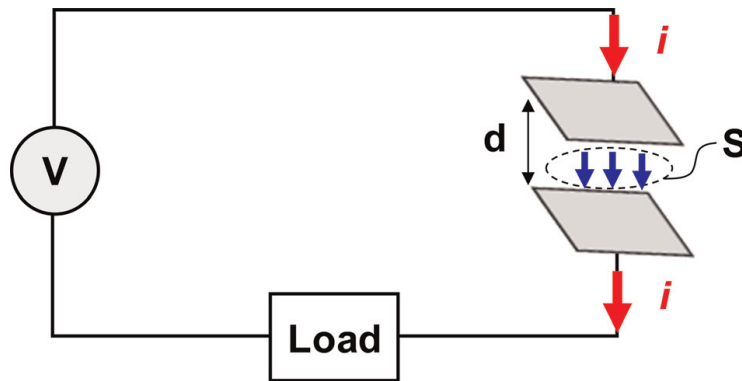


Figure 7.
Diagram of displacement current.

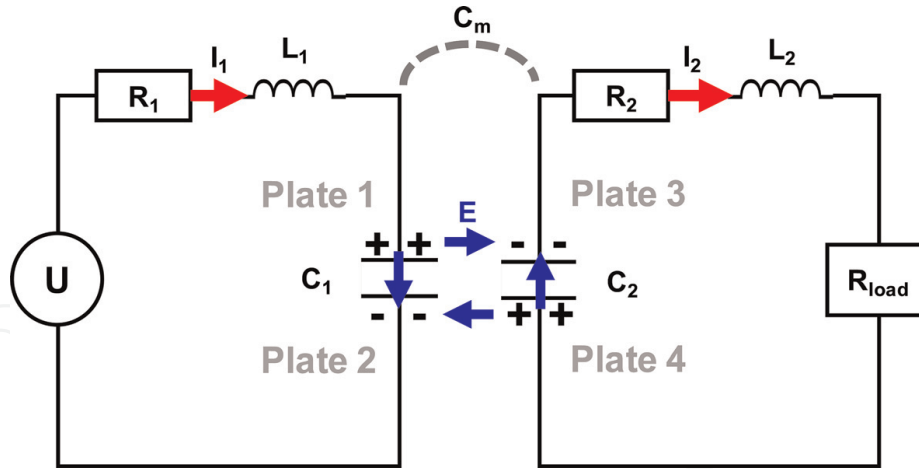


Figure 8.
 Circuit topology of electric field coupling with resonance.

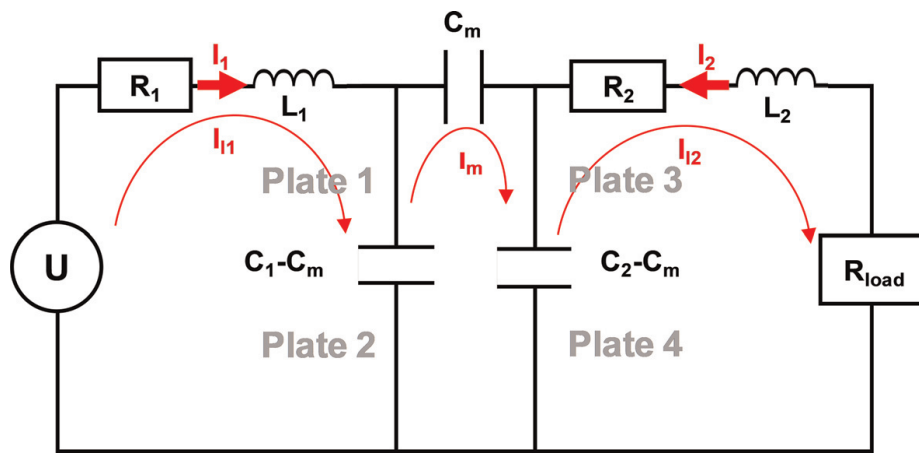


Figure 9.
 π -type equivalent circuit for electric field coupling with resonance.

$$Z_{in2} = \frac{1}{j\omega C_2 + \frac{1}{R_2 + j\omega L_2 + R_L}} \quad (39)$$

$$Z_2 = \frac{1}{\omega^2 C_m^2 Z_{in2}} \quad (40)$$

$$Z_{in1} = \frac{1}{j\omega C_1 + \frac{1}{Z_2}} + j\omega L_1 + R_1 \quad (41)$$

To analyze the input impedance, the extended π -type circuit with a separate capacitance is shown in **Figure 10**. The input impedance of each stage can be expressed as Eqs. (38), (39), and (40).

When operating frequency is equal to the resonant frequency on the secondary side, the imaginary part of the Z_{in2} becomes zero. Then, the resonant frequency can be acquired as Eq. (42).

$$\omega_2 = \sqrt{\frac{1}{L_2 C_2} - \left(\frac{R_2 + R_L}{L_2}\right)^2} \quad (42)$$

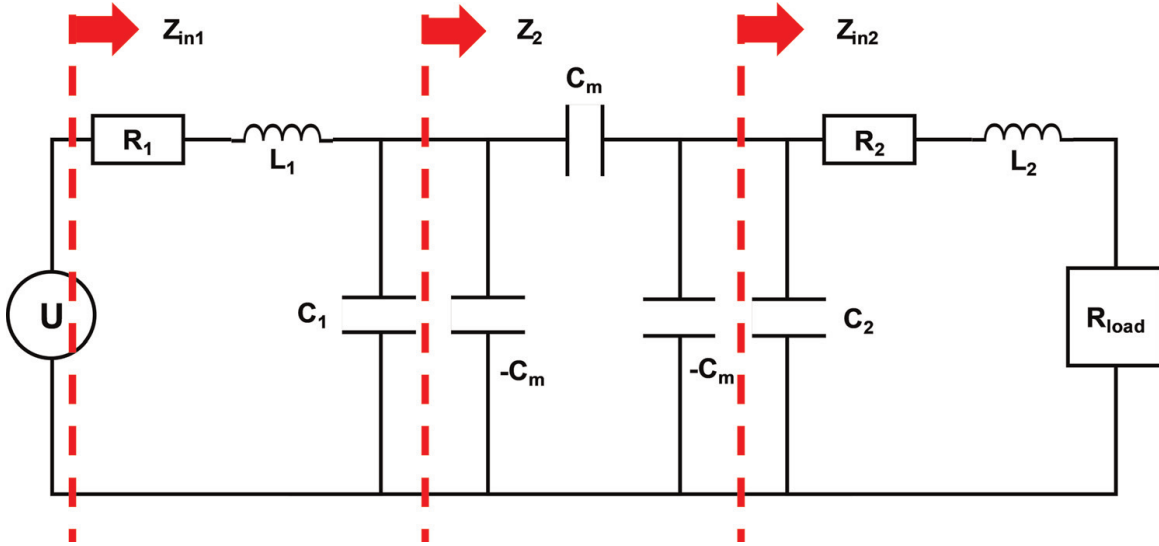


Figure 10.
 π -type circuit with a separate capacitance for electric field coupling with resonance.

In the same way, when the operating frequency is equal to the resonant frequency on the primary side, the imaginary part of the Z_{in1} becomes zero. The L_1 can be obtained as Eq. (43).

$$L_1 = \frac{C_1(R_2 + R_L)^2 - \omega_1^2 \left\{ C_2 \left[(R_2 + R_L)^2 + (\omega L_2)^2 \right] - L_2 \right\} \left\{ L_2 C_1 - (C_1 C_2 - C_m^2) \left[(R_2 + R_L)^2 + (\omega L_2)^2 \right] \right\}}{\omega_1^4 \left\{ L_2 C_1 - (C_1 C_2 - C_m^2) \left[(R_2 + R_L)^2 + (\omega L_2)^2 \right] \right\}^2 + \omega_1^2 C_1^2 (R_2 + R_L)^2} \quad (43)$$

To understand the power efficiency, the ratio of energy loss for the primary-side internal resistance, secondary-side internal resistance, and load can be denoted by P_{R1} , P_{R2} , and P_{RL} as Eq. (44).

$$P_{R_1} : P_{R_2} : P_{R_L} = |I_1|^2 R_1 : |I_2|^2 R_2 : |I_2|^2 R_L \quad (44)$$

The square ratio of I_2 and I_1 can be calculated as Eq. (45), according to Eq. (38) [16].

$$\left| \frac{I_1}{I_2} \right|^2 = \frac{\omega^2 C_1 C_2 \left[(R_2 + R_L)^2 + (\omega L_2)^2 \right] + C_1^2 (1 - \omega^2 L_2 C_2)}{C_m^2} \quad (45)$$

The power ratio can be rewritten as Eq. (46), according to Eqs. (44) and (45).

$$P_{R_1} : P_{R_2} : P_L = \left\{ \omega^2 C_1 C_2 \left[(R_2 + R_L)^2 + (\omega L_2)^2 \right] + C_1^2 (1 - \omega^2 L_2 C_2) \right\} R_1 : \{ C_m^2 \} R_2 : \{ C_m^2 \} R_L \quad (46)$$

Finally, the power efficiency can be expressed as Eq. (47).

$$\eta(\omega) = \frac{P_L}{P_{in}} = \frac{P_L}{P_{R_1} + P_{R_2} + P_L}$$

$$= \frac{\{C_m^2\}R_L}{\left\{\omega^2 C_1 C_2 \left[(R_2 + R_L)^2 + (\omega L_2)^2 \right] + C_1^2 (1 - \omega^2 L_2 C_2) \right\} R_1 + \{C_m^2\} R_2 + \{C_m^2\} R_L}$$

(47)

5. WPT system overview

The basic topology of magnetic field resonant coupling is shown in **Figure 11** [16, 20, 21]. The transmitter and receiver sides are coupled through the magnetic field (**Figure 11a**) and electric field (**Figure 11b**). The DC power supply generates the source power. The inverter is responsible for DC/AC conversion to produce the high-frequency AC power. The AC power is transferred to the receiver side and converted from AC to DC power by a rectifier. Then, the power is transferred to the load. In the WPT operating frequency for implantable devices, the common frequency is at a low frequency because of the reduction of tissue heating effect [22]. The typical frequency is 13.56 MHz within the license-free industrial, scientific, and medical (ISM) band [23].

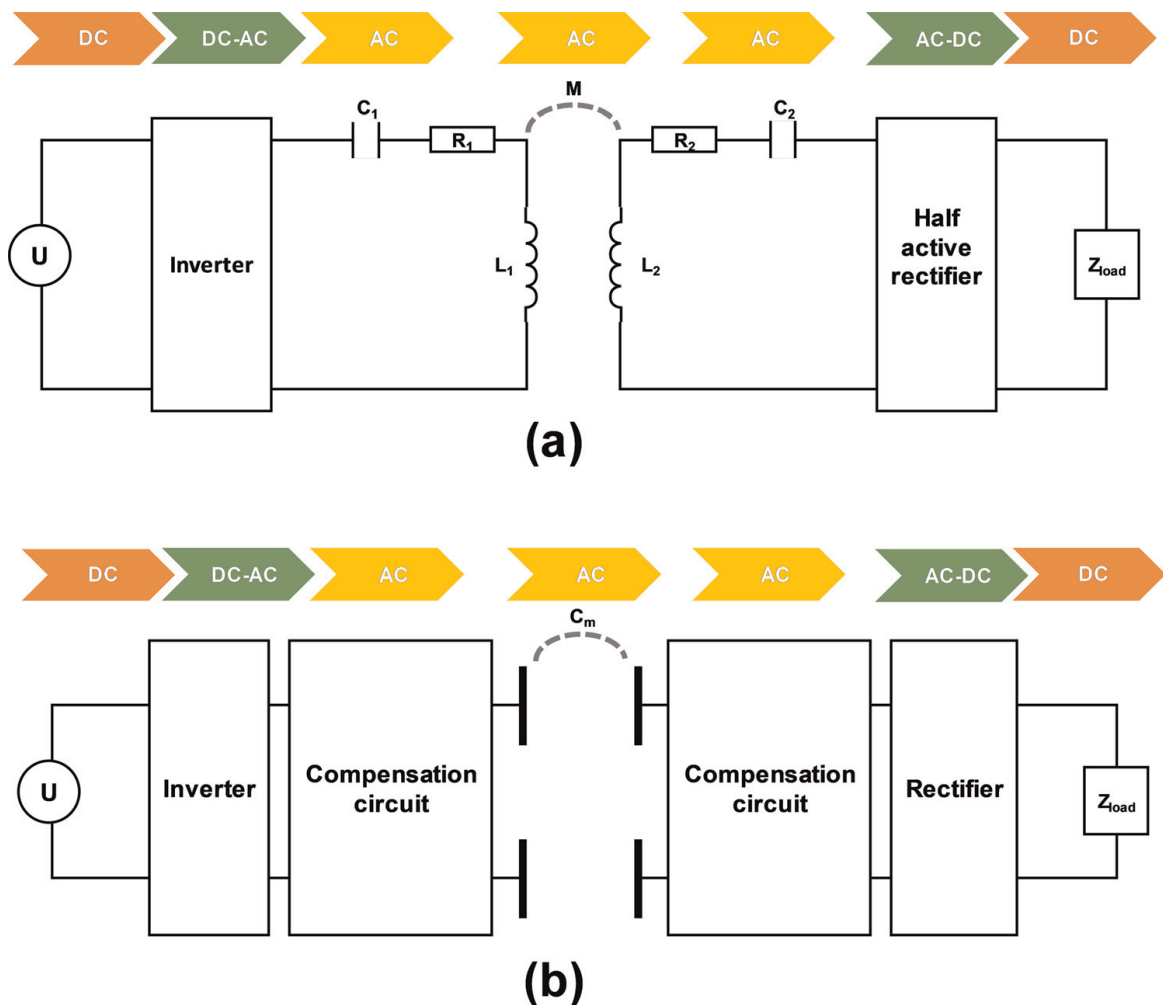


Figure 11. System overview for (a) magnetic field coupling and (b) electric field coupling methods.

The class E power amplifier is commonly applied in MHz-range WPT applications because of its excellent power efficiency from the properties of zero voltage switching and zero voltage derivative switching [24]. The class-E power amplifier can be depicted in **Figure 12**. In theory, it has a maximum efficiency of 100% [25], according to Eq. (48). The overall circuit consists of the power supply V_{dc} , RF-chuck, and passive load network. The RF-chuck with high reactance ensures DC voltage pass through the system. The passive load network is responsible for minimizing the overlap between drain voltage and drain current and further reducing the output power loss [26].

$$P_{\text{dissipation}} = \frac{1}{T_0} \int_{T_0} I_{DS} * V_{DS} dt = 0 \quad (48)$$

Some group has proposed a class E power amplifier-based WPT system for implantable biomedical in practical applications. Mutashar *et al.* [27] designed a wireless magnetic resonant coupling system using a class-E power amplifier and inductive power links via two spiral transmitters and receiver coils (**Figure 13a**). The 13.56 MHz carrier frequency within the ISM band range was selected to avoid tissue damage. The proposed class-E power amplifier can reach up to 87.2% power efficiency. The overall inductive coupling system achieves a power transmission efficiency of 73%. The compact structure could be implemented in bio-implants in the future. In practical applications for the electrical field coupling method, Narayanamoorthi *et al.* [24] developed a class-E-based capacitive coupled wireless power transfer system for biomedical implants (**Figure 13b**). They optimize the class E-based capacitive coupling WPT systems at an operating frequency of 13.56 MHz. Moreover, the matching circuit consisted of inductive-capacitive-inductive (LCL) impedance was used to improve the power efficiency of the power amplifier up to 96.34%.

6. WPT in emerging biomedical topics

WPT systems are rapidly evolving for biomedical implants, including emerging topics of implantable pacemaker devices, implantable optogenetic devices, and implantable impedance plethysmography (IPG).

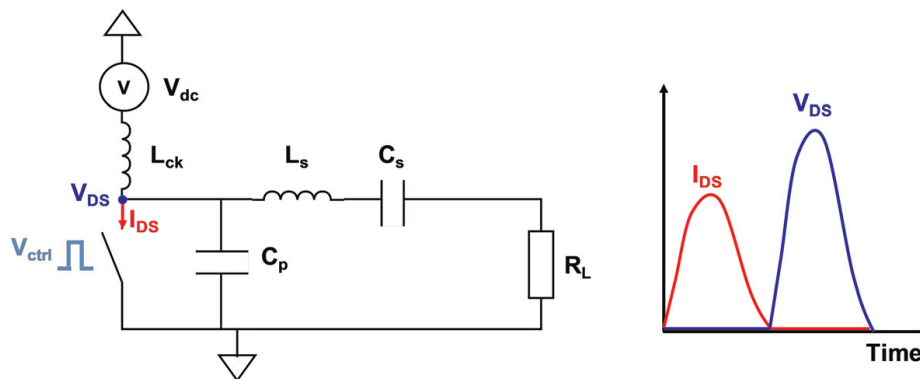


Figure 12.
Circuit diagram of a class E power amplifier.

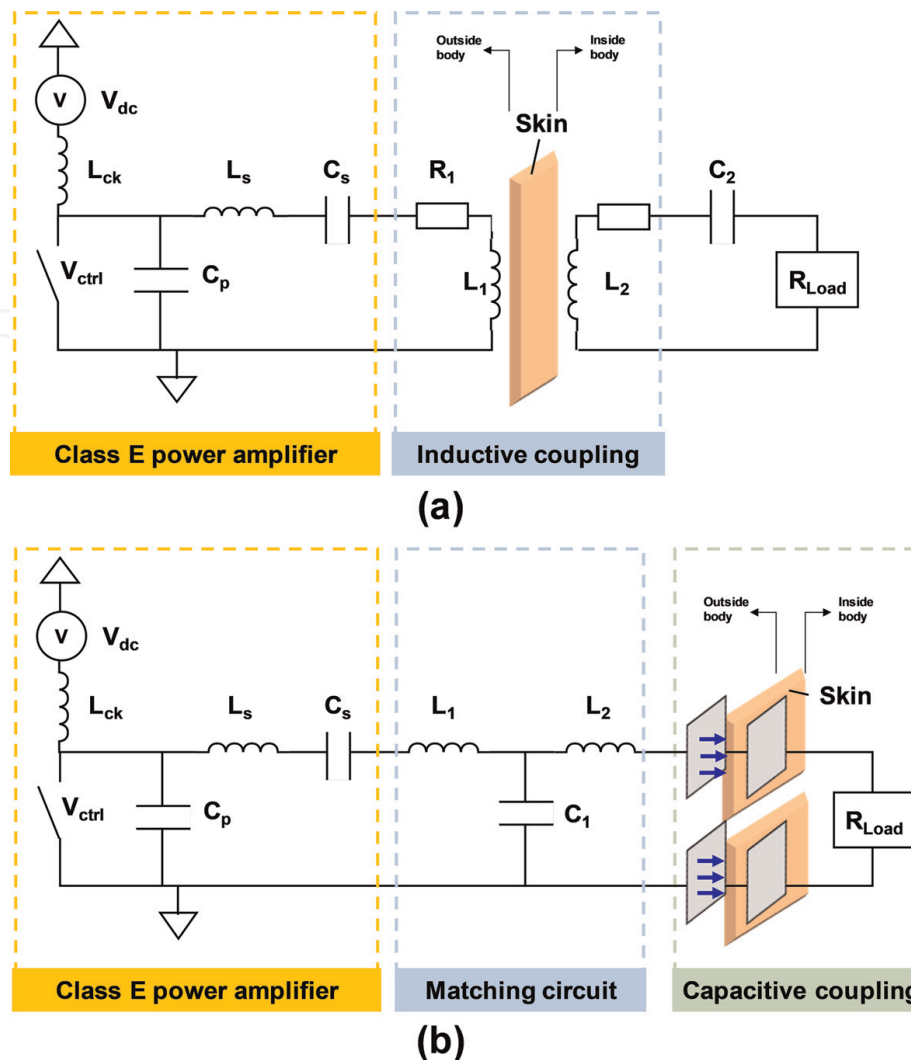


Figure 13. WPT system by (a) magnetic field coupling [27] and (b) electric field coupling for implantable applications [24].

6.1 Wireless charge-based implantable pacemaker

Heart failure is one of the most killers worldwide. It occupies one-third of all global death. Nowadays, the implantable cardioverter pacemaker is a common approach to directly suppress heart failure [28, 29]. However, the battery life could cause health risks and patient inconvenience. Parinaz Abiri *et al.* [30] developed an inductively powered wireless pacing device to realize remote cardiac stimulation. They designed a Class E-based magnetic field resonant coupling system with a resonant frequency of 13.56 MHz to pace rhythm on Yucatan miniature pig.

6.2 WPT-based implantable optogenetic device

Optogenetics is an emerging field that provides an alternative for direct electrical stimulation to modulate membrane voltage. By genetic modification, the ion channels in the cell can be sensitive to certain wavelengths of light [31]. Nowadays, several advanced biomedical topics have involved the optogenetic topic in different applications, including neuroscience to control animal behavior [32, 33] and cardiology to find out a solution for cardiovascular disease [34, 35]. Yu *et al.* [36] implement an

implantable optogenetic device implanted into the dog's chest. WPT-based optogenetic modulation of cardiac sympathetic nerve activity can prevent ventricular arrhythmias.

6.3 WPT-based implantable bio-impedance sensor

Bio-impedance sensing is a noninvasive sensing technology based on Ohm's law. It was commonly applied to cell structural depiction, human composition, and physiological measurement [37–40]. The main advantage of bio-impedance sensing is providing wearable and low-cost applications in biomedical engineering. The bio-impedance technique commonly uses the two-pair electrodes to detect arterial pulsation by Ohm's law. One pair of electrodes is responsible for current excitation in our body. Furthermore, the other pair electrodes are responsible for sensing voltage signals. Theodor *et al.* [41] developed an implantable bio-impedance sensor to measure the artery activity from the domestic pig for additional cardiovascular parameters extraction such as pulse rate and blood pressure [42].

7. Conclusion

This chapter has presented the WPT methodology for implantable medical devices. The common configuration of WPT and its principle were demonstrated, including magnetic field coupling and electric field coupling. Most of all, the recent emerging biomedical topics such as wireless-charging pacemakers, implantable optogenetic devices, and implantable bio-impedance sensors were demonstrated. Overall, this chapter thoroughly presented the electric principle of WPT and extended it to emerging biomedical applications.

IntechOpen

IntechOpen

Author details

Ting-Wei Wang^{1,2} and Ting-Tse Lin^{3,4,5,6*}

1 Department of Electrical Engineering, California Institute of Technology, Pasadena, CA, USA

2 Department of Medical Engineering, California Institute of Technology, Pasadena, CA, USA

3 Division of Cardiology, Department of Internal Medicine, National Taiwan University Hospital, Taipei, Taiwan


4 Cardiovascular Center, National Taiwan University Hospital Hsinchu Branch, Hsinchu, Taiwan

5 College of Medicine, National Taiwan University, Taipei, Taiwan

6 Division of Cardiology, Department of Internal Medicine, National Taiwan University Hospital Hsinchu Branch, Hsinchu, Taiwan

*Address all correspondence to: ttlin111@gmail.com

IntechOpen

© 2022 The Author(s). Licensee IntechOpen. This chapter is distributed under the terms of the Creative Commons Attribution License (<http://creativecommons.org/licenses/by/3.0>), which permits unrestricted use, distribution, and reproduction in any medium, provided the original work is properly cited. 

References

- [1] Sun L, Ma D, Tang H. A review of recent trends in wireless power transfer technology and its applications in electric vehicle wireless charging. *Renewable and Sustainable Energy Reviews*. 2018;**91**:490-503. DOI: 10.1016/j.rser.2018.04.016
- [2] Bi Z, Kan T, Mi CC, Zhang Y, Zhao Z, Keoleian GA. A review of wireless power transfer for electric vehicles: Prospects to enhance sustainable mobility. *Applied Energy*. 2016;**179**:413-425. DOI: 10.1016/j.apenergy.2016.07.003
- [3] Hoang H, Lee S, Kim Y, Choi Y, Bien F. An adaptive technique to improve wireless power transfer for consumer electronics. *IEEE Transactions on Consumer Electronics*. 2012;**58**(2): 327-332. DOI: 10.1109/TCE.2012.6227430
- [4] Kiani M, Ghovanloo M. An RFID-based closed-loop wireless power transmission system for biomedical applications. *IEEE Transactions on Circuits and Systems II: Express Briefs*. 2010;**57**(4):260-264. DOI: 10.1109/TCSII.2010.2043470
- [5] Iqteit N, Yahya K, Khan SA. Wireless power charging in electrical vehicles. In: Zellagui M, editor. *Wireless Power Transfer. Recent Development, Applications and New Perspectives*. London, UK: IntechOpen; 2021
- [6] Meng E, Sheybani R. Insight: Implantable medical devices. *Lab on a Chip*. 2014;**14**(17):3233-3240. DOI: 10.1039/C4LC00127C
- [7] Basar MR, Ahmad MY, Cho J, Ibrahim F. Application of wireless power transmission systems in wireless capsule endoscopy: An overview, *Sensors (Basel, Switzerland)*. 2014;**14**(6):10929-10951. DOI: 10.3390/s140610929
- [8] DeForge WF. Cardiac pacemakers: A basic review of the history and current technology. *Journal of Veterinary Cardiology: the Official Journal of the European Society of Veterinary Cardiology*. 2019;**22**:40-50. DOI: 10.1016/j.jvc.2019.01.001
- [9] Wang T-W, Lin T-T. Electromagnetic compatibility issues in medical devices. In: Kishk A, editor. *Electromagnetic Compatibility*. London, UK: IntechOpen; 2021
- [10] Kanaan AI, Sabaawi AM. Implantable wireless systems: A review of potentials and challenges. In: Al-Rizzo H, Abushamleh S, editors. *Antenna Systems*. London, UK: IntechOpen; 2021
- [11] Shadid R, Noghianian S. A literature survey on wireless power transfer for biomedical devices. *International Journal of Antennas and Propagation*. 2018;**2018**:4382841. DOI: 10.1155/2018/4382841
- [12] Khan SR, Pavuluri SK, Cummins G, Desmulliez MPY. Wireless power transfer techniques for implantable medical devices: A review. *Sensors*. 2020;**20**(12):3487. DOI: 10.3390/s20123487
- [13] Etemadrezai M. Wireless power transfer. In: Rashid MH, editor. *Power Electronics Handbook*. 4th ed. Oxford, UK: Butterworth-Heinemann; 2018. pp. 711-722
- [14] Garnica J, Chinga RA, Lin J. Wireless power transmission: From far field to near field. *Proceedings of the IEEE*. 2013;**101**(6):1321-1331. DOI: 10.1109/JPROC.2013.2251411
- [15] Wang TW, Sung YL, Lin SF. Cardiac influence of repetitive transcranial magnetic stimulation in small animals.

IEEE Journal of Electromagnetics, RF and Microwaves in Medicine and Biology. 2020;4(4):279-285.

DOI: 10.1109/JERM.2019.2958686

[16] Imura T. Wireless Power Transfer: Using Magnetic and Electric Resonance Coupling Techniques. Singapore: Springer Nature; 2020

[17] Wang TW, Zhang H, Lin SF. Influence of capacitive coupling on high-fidelity non-contact ECG measurement. IEEE Sensors Journal. 2020;20(16): 9265-9273. DOI: 10.1109/JSEN.2020.2986723

[18] Wang TW, Lin SF. Negative impedance capacitive electrode for ECG sensing through fabric layer. IEEE Transactions on Instrumentation and Measurement. 2021;70:1-8.

DOI: 10.1109/TIM.2020.3045187

[19] Wang T-W, Lin S-F. Non-contact capacitive sensing for ECG recording in small animals. Measurement Science and Technology. 2020;31(12):125703. DOI: 10.1088/1361-6501/ab8cfc

[20] Kindl V, Zavrel M, Drabek P, Kavalir T. High efficiency and power tracking method for wireless charging system based on phase-shift control. Energies. 2018;11(8):2065. Available from: <https://www.mdpi.com/1996-1073/11/8/2065>

[21] Yi K. Capacitive coupling wireless power transfer with quasi-LLC resonant converter using electric vehicles' windows. Electronics. 2020;9(4):676. DOI: 10.3390/electronics9040676

[22] Freeman DK, Byrnes SJ. Optimal frequency for wireless power transmission into the body: Efficiency versus received power. IEEE Transactions on Antennas and

Propagation. 2019;67(6):4073-4083. DOI: 10.1109/TAP.2019.2905672

[23] Sanchez-Montero R, Lopez-Espi P-L, Alen-Cordero C, Martinez-Rojas J-A. Bend and moisture effects on the performance of a U-shaped slotted wearable antenna for off-body communications in an Industrial Scientific Medical (ISM) 2.4 GHz band. Sensors. 2019;19(8):1804. DOI: 10.3390/s19081804

[24] Narayanamoorthi R, Vimala Juliet A, Chokkalingam B, Padmanaban S, Leonowicz ZM. Class E power amplifier design and optimization for the capacitive coupled wireless power transfer system in biomedical implants. Energies. 2017;10(9): 1409. DOI: 10.3390/en10091409

[25] Lim A, Tan A, Kong Z-H, Ma K. A design methodology and analysis for transformer-based Class-E power amplifier. Electronics. 2019;8(5):494. DOI: 10.3390/electronics8050494

[26] Sokal NO, Sokal AD. Class E-A new class of high-efficiency tuned single-ended switching power amplifiers. IEEE Journal of Solid-State Circuits. 1975; 10(3):168-176. DOI: 10.1109/JSSC.1975.1050582

[27] Mutashar S. Efficiency improvement of wireless power transmission for bio-implanted devices. International Journal of Biomedical Engineering. 2013;7: 721-724

[28] Kirk JA et al, Pacemaker-induced transient asynchrony suppresses heart failure progression, Science Translational Medicine. 2015;7(319): 319ra207. DOI: 10.1126/scitranslmed.aad2899

[29] Khazanie P, Hellkamp AS, Fonarow GC, Curtis LH, Al-Khatib SM,

- Hernandez AF. Permanent pacemaker use among patients with heart failure and preserved ejection fraction: Findings from the Acute Decompensated Heart Failure National Registry (ADHERE) National Registry. *American Heart Journal*. 2018;**198**:123-128. DOI: 10.1016/j.ahj.2017.12.020
- [30] Abiri P et al. Inductively powered wireless pacing via a miniature pacemaker and remote stimulation control system. *Scientific Reports*. 2017;**7**(1):6180. DOI: 10.1038/s41598-017-06493-5
- [31] Deisseroth K. Optogenetics. *Nature Methods*. 2011;**8**(1):26-29. DOI: 10.1038/nmeth.f.324
- [32] Mahmoudi P, Veladi H, Pakdel FG. Optogenetics, tools and applications in neurobiology. *Journal of Medical Signals and Sensors*. 2017;**7**(2):71-79
- [33] Boyden ES. Optogenetics and the future of neuroscience. *Nature Neuroscience*. 2015;**18**(9):1200-1201. DOI: 10.1038/nn.4094
- [34] Williams JC, Entcheva E. Optogenetic versus electrical stimulation of human cardiomyocytes: Modeling insights. *Biophysical Journal*. 2015; **108**(8):1934-1945. DOI: 10.1016/j.bpj.2015.03.032
- [35] Entcheva E, Kay MW. Cardiac optogenetics: A decade of enlightenment. *Nature Reviews Cardiology*. 2021;**18**(5):349-367. DOI: 10.1038/s41569-020-00478-0
- [36] Yu L et al. Optogenetic modulation of cardiac sympathetic nerve activity to prevent ventricular arrhythmias. *Journal of the American College of Cardiology*. 2017;**70**(22):2778-2790. DOI: 10.1016/j.jacc.2017.09.1107
- [37] Wang TW, Chen WX, Chu HW, Lin SF. Single-channel bioimpedance measurement for wearable continuous blood pressure monitoring. *IEEE Transactions on Instrumentation and Measurement*. 2021;**70**:1-9. DOI: 10.1109/TIM.2020.3035578
- [38] Wang TW et al. Single-channel impedance plethysmography neck patch device for unobtrusive wearable cardiovascular monitoring. *IEEE Access*. 2020;**8**:184909-184919. DOI: 10.1109/ACCESS.2020.3029604
- [39] Wang T-W et al. Bio-impedance measurement optimization for high-resolution carotid pulse sensing. *Sensors*. 2021;**21**(5):1600. DOI: 10.3390/s21051600
- [40] Wang TW, Sung YL, Chu HW, Lin SF. IPG-based field potential measurement of cultured cardiomyocytes for optogenetic applications. *Biosensors & Bioelectronics*. 2021;**179**:113060. DOI: 10.1016/j.bios.2021.113060
- [41] Theodor M et al. Implantable impedance plethysmography. *Sensors*. 2014;**14**(8):14858-14872. DOI: 10.3390/s140814858
- [42] Wang TW, Lin SF. Wearable piezoelectric-based system for continuous beat-to-beat blood pressure measurement. *Sensors (Basel, Switzerland)*. 2020;**20**(3):851. DOI: 10.3390/s20030851